Hyperfine interaction and electron-spin decoherence in graphene and carbon nanotube quantum dots

Jan Fischer,[1] Björn Trauzettel,[2] and Daniel Loss[1]
[1]*Department of Physics, University of Basel, Klingelbergstrasse 82, 4056 Basel, Switzerland*
[2]*Institute of Theoretical Physics and Astrophysics, University of Würzburg, D-97074 Würzburg, Germany*
(Received 19 June 2009; revised manuscript received 4 September 2009; published 1 October 2009)

We analytically calculate the nuclear-spin interactions of a single electron confined to a carbon nanotube or graphene quantum dot. While the conduction-band states in graphene are *p*-type, the accordant states in a carbon nanotube are *sp*-hybridized due to curvature. This leads to an interesting interplay between isotropic and anisotropic hyperfine interactions. By using only analytical methods, we are able to show how the interaction strength depends on important physical parameters, such as curvature and isotope abundances. We show that for the investigated carbon structures, the ^{13}C hyperfine coupling strength is less than 1 μeV, and that the associated electron-spin decoherence time can be expected to be several tens of microseconds or longer, depending on the abundance of spin-carrying ^{13}C nuclei. Furthermore, we find that the hyperfine-induced Knight shift is highly anisotropic, both in graphene and in nanotubes of arbitrary chirality.

DOI: 10.1103/PhysRevB.80.155401 PACS number(s): 03.65.Yz, 72.25.Rb, 73.21.La, 31.30.Gs

I. INTRODUCTION

The spin of an electron confined to a semiconductor quantum dot is a prime candidate for quantum information processing devices, with potential applications in spintronics[1–3] and quantum computation.[4–6] Schemes for quantum computation rely on a sufficiently long lifetime of initialized spin states. One major problem is that the electron is not isolated from its environment but interacts with the nuclei in the semiconductor it has been confined to. This interaction leads to relaxation of excited spin states, as well as to the decay of spin-state superpositions (decoherence). For most quantum dots at low temperatures, the main source of spin decoherence is the electron's interaction with a fluctuating magnetic field created by the randomly precessing nuclear spins.[7–13] For III-V semiconductor quantum dots, with their high abundance of spin-carrying nuclear isotopes, the associated decoherence times are quite short, usually of order nanoseconds,[8–10,14] if no manipulations on the nuclear system are performed.

One way of overcoming the problem of short decoherence times is to build quantum dots from semiconductors with lower abundances of spin-carrying isotopes, potentially resulting in weaker nuclear-spin interactions. Carbon structures naturally consist of 99% ^{12}C with nuclear-spin 0 and only of 1% ^{13}C with nuclear-spin $\frac{1}{2}$, and are therefore promising materials for building quantum dots featuring long spin decoherence times. This extraordinary property of carbon materials, as well as their comparatively weak spin-orbit interactions, has led to proposals of fabricating quantum dots in graphene ribbons with armchair boundaries[15] and in carbon nanotubes (CNTs).[16]

Although it was not yet possible to experimentally realize a single-electron quantum dot in graphene, Coulomb-blockade measurements in gated graphene quantum dots have already been carried out successfully.[17,18] Experiments on single electrons in CNTs have advanced even more.[19–33] Very recently, first measurements on nuclear-spin interactions and electron-spin dynamics in CNTs have been performed,[34,35] reporting an unexpectedly strong hyperfine interaction of order $A \simeq 100$ μeV in ^{13}C-enriched CNTs (we will comment on the discrepancy between this result and our calculations in Sec. VI). Furthermore, theoretical and experimental NMR studies on fullerenes[36] have been carried out as well as *ab initio* calculations on hyperfine interaction in small graphene flakes.[37] An analytical investigation of nuclear-spin interactions of electrons confined to graphene and CNTs, however, has so far been missing.

In our work, we analytically calculate the interaction of a single electron confined to a graphene ribbon or a CNT (see Fig. 1) with the spins of the surrounding ^{13}C nuclei. For CNTs we find an interesting interplay between isotropic and anisotropic hyperfine interactions which depends on the CNT geometry and which leads to a highly anisotropic Knight shift and an unusual alignment of the nuclear spins around a CNT circumference (in the ground state). Furthermore, we calculate the decoherence dynamics of the electron spin and

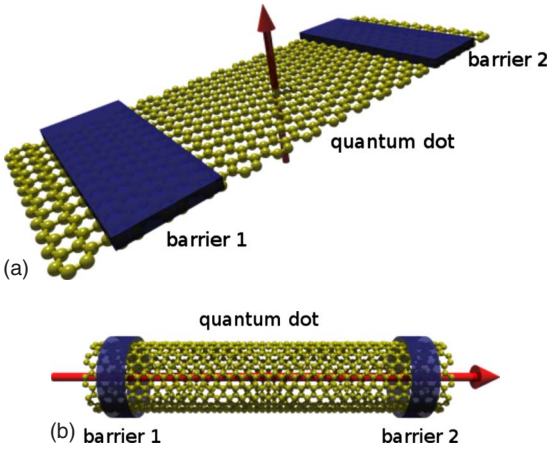

FIG. 1. (Color online) Sketch of the systems under consideration throughout this work: (a) a single electron confined to a quantum dot defined by two barriers on a graphene ribbon; (b) a single-electron quantum dot defined in a carbon nanotube. Externally applied magnetic fields are indicated by the red arrows.

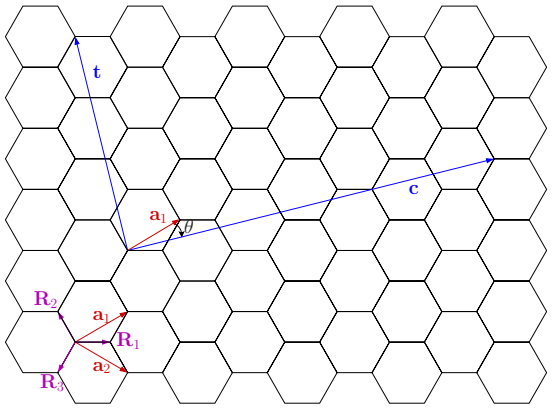

FIG. 2. (Color online) Definitions used throughout this work: $\mathbf{a}_1$ and $\mathbf{a}_2$ denote the basis vectors of the honeycomb lattice, $\mathbf{R}_j$ are the relative nearest-neighbor positions, $\mathbf{c}$ and $\mathbf{t}$ are the circumferential and transverse vectors, respectively, and $\theta=\theta_{nm}$ is the chiral angle between $\mathbf{c}$ and $\mathbf{a}_1$.

find that, even without manipulating the nuclear spins, the hyperfine-associated decoherence times can be on the order of tens of microseconds or longer, depending on the relative abundance of ^{13}C nuclei. These time scales are much longer than the ones typically found for III-V semiconductor quantum dots, making carbon-based quantum dots promising spin-qubit candidates.

Our paper is organized as follows: in Sec. II we determine the wave function of a conduction-band electron in a CNT. In Sec. III we derive an effective Hamiltonian for the nuclear-spin interactions and find a highly anisotropic coupling of the electron to the ^{13}C nuclear spins, which results in an anisotropic Knight shift and an unusual alignment of the nuclear spins around the nanotube, as shown in Sec. IV. In Sec. V, we determine the electron-spin dynamics and the associated spin decoherence times. We give a detailed comparison of our results with previous studies on comparable systems in Sec. VI, and conclude in Sec. VII.

II. BONDS AND BANDS

The carbon atom features six electrons: two core electrons and four valence electrons. In a solid, the four valence electrons (which are in $2s$ and $2p$ states) form the bonds with the nearest-neighbor atoms. In two-dimensional graphite, or graphene, each atom has three nearest neighbors, and three of the four valence electrons form sp^2-hybridized bonds (called σ bonds) with those neighbors, while the fourth electron is in a so-called π state perpendicular to the σ bonds.[38] The π electrons in graphene determine the band structure near the Fermi energy, while the σ electrons form more remote bands. A conduction-band electron is therefore in a π state.

A CNT can be regarded as a graphene sheet that had been rolled up along some direction $\mathbf{c}$, defining a symmetry axis $\mathbf{t}$ of the CNT. The circumferential and translational vectors are defined in terms of the basis vectors $\mathbf{a}_1$ and $\mathbf{a}_2$ as (see Fig. 2)

$$\mathbf{c} = n\mathbf{a}_1 + m\mathbf{a}_2, \quad \mathbf{t} = t_1\mathbf{a}_1 + t_2\mathbf{a}_2. \tag{1}$$

Here, $n,m \in \mathbb{N}_0$ are the chiral indices, and $t_1=(2m+n)/d_R$, $t_2=-(2n+m)/d_R$ with d_R being the greatest common divisor of $2n+m$ and $2m+n$. We denote the chiral angle between $\mathbf{c}$ and $\mathbf{a}_1$ by $\theta=\theta_{nm}$.

The curvature of the CNT causes a geometrical tilting of the σ bonds which results in an sp hybridization of the conduction-band states. In Ref. 39, this effect has been studied perturbatively in lowest order in the small parameter $2\pi/L$, where $L=\sqrt{n^2+nm+m^2}$ is the circumference of the CNT in units of the lattice constant $a \simeq 2.5$ Å.[54]

The wave function of a conduction-band electron in a periodic crystal is given by Bloch's theorem: $\Psi_{\mathbf{k}\sigma} = \frac{1}{\sqrt{N_A}} e^{i\mathbf{k}\cdot\mathbf{r}} u_{\mathbf{k}\sigma}(\mathbf{r})$, where N_A is the number of atomic sites in the crystal and the Bloch amplitude $u_{\mathbf{k}\sigma}(\mathbf{r})$ has the periodicity of the lattice. Following Ref. 40, we approximate the Bloch amplitude $u_{\mathbf{k}\sigma}(\mathbf{r})$ at the K and K' points by a linear combination of hydrogenic orbitals, $u_\sigma(\mathbf{r})=\Sigma_{\mathbf{R}}\pi(\mathbf{r}-\mathbf{R})$, where[39]

$$\pi(\mathbf{r}) = N_{nm}\left\{\psi_{2p_\perp}(\mathbf{r}) + \frac{\pi}{2\sqrt{3}L}[\psi_{2s}(\mathbf{r}) + \sin(3\theta'_{nm})\psi_{2p_t}(\mathbf{r}) + \cos(3\theta'_{nm})\psi_{2p_c}(\mathbf{r})]\right\}, \tag{2}$$

and the sum runs over all lattice sites in the CNT. In the above, ψ_{2s} represents a hydrogenic $2s$ orbital, ψ_{2p_t}, ψ_{2p_c}, and $\psi_{2p_\perp}$ are, respectively, the $2p$ orbitals along the transverse, circumferential, and radial direction of the CNT, and N_{nm} normalizes the Bloch amplitude to two atoms per unit cell. θ'_{nm} is the angle between $\mathbf{c}$ and $\mathbf{R}_1$, and we can write $\sin(3\theta'_{nm})=(n-m)(2n^2+5nm+2m^2)/2L^3$ and $\cos(3\theta'_{nm}) = 3\sqrt{3}nm(n+m)/2L^3$ in terms of the chiral indices.[39] The hydrogenic orbitals consist of a radial and an angular part, e.g., $\psi_{2s}(\mathbf{r})=R_{20}(r)Y_0^0(\vartheta,\varphi)$. We will choose a local coordinate system at each lattice site, such that ψ_{2p_t}, ψ_{2p_c}, and $\psi_{2p_\perp}$ correspond to hydrogenic $2p$ orbitals in z, y, and x direction, respectively (see below). The radial components of the hydrogenic orbitals depend on an effective screened nuclear charge Z_{eff} "seen" by the electron.[41]

Our choice of the Bloch amplitude implicitly assumes that the electron is tightly bound to the nuclei, i.e., that the radial component of $\pi(\mathbf{r})$ drops off fast on the scale of the nearest-neighbor distance. We have estimated that $|\pi(\mathbf{r}+\mathbf{R}_{\text{n.n.}})|^2/|\pi(\mathbf{r})|^2 \simeq 10^{-3}$ for any nearest-neighbor lattice vector $\mathbf{R}_{\text{n.n.}}$, justifying our assumption.

In a quantum dot, the electron is delocalized over many lattice sites and its Bloch amplitude is modulated by an envelope-function Φ_σ defined by the confinement potential (see Ref. 16 for the envelope function of a quantum dot defined by a rectangular confinement potential in a semiconducting CNT). Including the spin states $|\sigma\rangle=|\uparrow,\downarrow\rangle$, we write the electron states as

$$|\Psi_\sigma\rangle = |\Phi_\sigma;u_\sigma\rangle|\sigma\rangle, \tag{3}$$

where, in the envelope-function approximation, $\langle\mathbf{r}|\Phi_\sigma;u_\sigma\rangle = \Phi_\sigma(\mathbf{r})u_\sigma(\mathbf{r})$. Since we did not include spin-orbit interactions in our model, the orbital wave function is independent of the spin state, and we may omit the subscript σ: $\Phi_\sigma(\mathbf{r}) = \Phi(\mathbf{r})$ and $u_\sigma(\mathbf{r})=u(\mathbf{r})$.

III. NUCLEAR-SPIN INTERACTIONS

A. Carbon nanotubes

There are three terms that couple the spin of the confined electron to the nuclear spins in the CNT: the Fermi contact interaction, the anisotropic hyperfine interaction and the coupling of electron orbital angular momentum to the nuclear spins. These interactions are represented by the Hamiltonians[42]

$$h_1^k = \frac{\mu_0}{4\pi}\frac{8\pi}{3}\gamma_S\gamma_{j_k}\delta(\mathbf{r}_k)\mathbf{S}\cdot\mathbf{I}_k, \tag{4}$$

$$h_2^k = \frac{\mu_0}{4\pi}\gamma_S\gamma_{j_k}\frac{3(\mathbf{n}_k\cdot\mathbf{S})(\mathbf{n}_k\cdot\mathbf{I}_k)-\mathbf{S}\cdot\mathbf{I}_k}{r_k^3(1+d/r_k)}, \tag{5}$$

$$h_3^k = \frac{\mu_0}{4\pi}\gamma_S\gamma_{j_k}\frac{\mathbf{L}_k\cdot\mathbf{I}_k}{r_k^3(1+d/r_k)}, \tag{6}$$

respectively, where $\gamma_S=2\mu_B$, $\gamma_{j_k}=g_{j_k}\mu_N$, μ_B is the Bohr magneton, g_{j_k} is the nuclear g factor of isotopic species j_k, μ_N is the nuclear magneton, μ_0 is the vacuum permeability, $\mathbf{r}_k=\mathbf{r}-\mathbf{R}_k$ is the electron-spin position operator relative to the kth nucleus, $d\simeq Z\times 1.5\times 10^{-15}$ m is a length of nuclear dimensions, Z is the charge of the nucleus, and $\mathbf{n}_k=\mathbf{r}_k/r_k$. $\mathbf{S}$ and $\mathbf{L}_k=\mathbf{r}_k\times\mathbf{p}$ denote the spin and orbital angular-momentum operators (with respect to the k^{th} nucleus) of the electron, respectively. The cutoff $1+d/r_k$ comes from the Dirac equation (see, e.g., Ref. 42) and avoids unphysical divergences from expectation values of the Hamiltonians h_2^k and h_3^k. In the problem considered here, this cutoff may be omitted for the following reasons: (i) the expectation values of h_2^k and h_3^k with respect to an s state vanish identically due to the spherical symmetry of the wave function and the vanishing orbital angular momentum, respectively. The expectation values with respect to a p state are nonzero, but the p-wave function goes to zero sufficiently fast at the position of each nucleus, thus avoiding a divergence. (ii) As mentioned above, the electron wave function does not extend significantly to the nearest-neighbor lattice sites. Hence, within our tight-binding approximation, the orbital $\pi(\mathbf{r})$ centered around some nucleus cannot cause a divergence at the position of a nearest neighbor.

We note that the orbital angular-momentum $\mathbf{L}_k$ which appears in Eq. (6) is associated with the electronic motion around the k^{th} nucleus and is described by the Bloch part of the electron wave function. On the other hand, it has been shown in Ref. 43, that interatomic currents can occur along the nanotube circumference to which another orbital angular-momentum $\mathcal{L}$ may be associated which is described by the envelope part of the electron wave function. However, the hyperfine coupling strength is defined via the Bloch part of the electron wave function and therefore a consideration of the coupling between the valley degrees of freedom via envelope-function-associated angular momenta is beyond the scope of the present work.

We will consider CNTs and graphene with different abundances of the nuclear isotopes ^{12}C and ^{13}C. While ^{12}C does not carry a nuclear spin, the nuclear gyromagnetic ratio of ^{13}C is nonvanishing and given by $\gamma_{^{13}\text{C}}=7.1\times 10^{-27}$ J/T.

The Fermi contact interaction (4) yields a finite contribution for s states, but vanishes for p states. The anisotropic hyperfine interaction (5) and the coupling of orbital angular momentum (6) vanish for s states because of their spherical symmetry and zero orbital angular momentum, but yield a finite contribution for p states. Therefore, when considering CNTs, all three interactions (4)–(6) have to be taken into account because of the sp-hybridized electron states (2), while for graphene, only the interactions (5) and (6) are relevant, due to the purely p-type wave function [corresponding to the limit $n,m\to\infty$ in Eq. (2)].

We first calculate matrix elements of the interactions (4)–(6) with respect to the electron wave function (3), which will lead to effective spin Hamiltonians and to the associated coupling strengths in the CNT case. Throughout this section, we will consider a CNT that consists only of spin-carrying ^{13}C isotopes. The possibility of different nuclear isotope abundances will then be taken into account in Sec. V. From the CNT results, it will be possible to perform the "graphene limit," which we postpone to Sec. III B.

We start with the Fermi contact interaction and calculate

$$\langle\Psi_\sigma|h_1^k|\Psi_{\sigma'}\rangle = \frac{2\mu_0\gamma_S\gamma_{^{13}\text{C}}}{3}\sum_k |u(\mathbf{r}_k)|^2|\Phi(\mathbf{r}_k)|^2\langle\sigma|\mathbf{S}\cdot\mathbf{I}_k|\sigma'\rangle, \tag{7}$$

assuming that the electron-spin density does not depend on the lattice site, which is justified if, e.g., the envelope-function $\Phi(\mathbf{r})$ describes the ground state of the quantum dot. The effects of a site dependence of the electron-spin density have been recently considered in Ref. 44. Evaluating the spin matrix elements leads to the following effective spin Hamiltonian:

$$H_1 = \sum_k A_k^{(1)}\mathbf{S}\cdot\mathbf{I}_k, \tag{8}$$

with coupling constants $A_k^{(1)}=A_1 v_0|\Phi(\mathbf{r}_k)|^2$ (where v_0 is the volume of a primitive unit cell) and the associated coupling strength

$$A_1 = \frac{\mu_0\gamma_S\gamma_{^{13}\text{C}}Z_{\text{eff}}^3}{3\pi a_0^3}N_{nm}^2\beta_{nm}^2, \tag{9}$$

where we have introduced $\beta_{nm}=\pi/2\sqrt{3}L$, and a_0 is the Bohr radius. The normalization factor N_{nm} can be determined by normalizing Eq. (2) to two atoms per unit cell

$$N_{nm} = 2\sqrt{\frac{L^2}{\pi^2+4L^2}}. \tag{10}$$

We have evaluated Eq. (9) for CNTs of different chiralities in Table I. For typical CNTs, the coupling strength A_1 is about three orders of magnitude smaller than that for an electron in a GaAs quantum dot ($A_1^{\text{GaAs}}\simeq 90$ μeV, see Ref. 45), for two reasons: (i) the hybridization prefactor $N_{nm}\beta_{nm}$ is on the order of 0.05 and enters quadratically into A_1. (ii) The effective nuclear charge (which enters in third power into A_1) is

TABLE I. Estimated hyperfine coupling strengths (in μeV) for nanotubes of different chiralities (n,m).

	(10,0)	(20,0)	(5,10)	(9,15)	(5,5)	(10,10)	(20,20)
A_1	0.19	0.05	0.12	0.05	0.26	0.07	0.02
A_2^x	0.59	0.60	0.59	0.60	0.58	0.60	0.61
A_2^y	−0.29	−0.30	−0.30	−0.30	−0.29	−0.30	−0.30
A_2^z	−0.30	−0.30	−0.30	−0.30	−0.30	−0.30	−0.30

$Z_{\text{eff}}^{\text{C}} \simeq 3.2$ for carbon, but $Z_{\text{eff}}^{\text{Ga}} \simeq 7.1$ for gallium and $Z_{\text{eff}}^{\text{As}} \simeq 8.9$ for arsenic.[41]

The sign of the isotropic interaction is positive for all nanotube diameters, in contrast to results reported previously,[46] where spin relaxation of conduction electrons has been calculated numerically and a sign change in the hyperfine coupling constant A_1 has been found for small nanotube diameters. This is due to the fact that in Ref. 46 the coupling of the $1s$ core electrons to the nuclear spins is included, which, however, is irrelevant for the hyperfine interaction of a conduction electron and, hence, for the electron spin dephasing considered in this article.

Now we look at the anisotropic hyperfine interaction. Due to symmetry, the s part of the hybridized wave function does not contribute. Taking matrix elements $\langle \Psi_\sigma | h_2^k | \Psi_{\sigma'} \rangle$ just like above, we arrive at an effective Hamiltonian

$$H_2 = \sum_k (A_k^{(2,x)} S^x I_k^x + A_k^{(2,y)} S^y I_k^y + A_k^{(2,z)} S^z I_k^z), \tag{11}$$

with coupling constants $A_k^{(2,j)} = A_2^j v_0 |\Phi(\mathbf{r}_k)|^2$ and the coupling strengths

$$A_2^j = \frac{\mu_0 \gamma_S \gamma^{13}_{\text{C}} Z_{\text{eff}}^3}{120\pi a_0^3} N_{nm}^2 \lambda_j, \tag{12}$$

where

$$\lambda_x = 1 - \frac{1}{2}\beta_{nm}^2, \tag{13}$$

$$\lambda_y = -\frac{1}{2} - \frac{1}{2}\beta_{nm}^2 \sin^2(3\theta'_{nm}) + \beta_{nm}^2 \cos^2(3\theta'_{nm}), \tag{14}$$

$$\lambda_z = -\frac{1}{2} + \beta_{nm}^2 \sin^2(3\theta'_{nm}) - \frac{1}{2}\beta_{nm}^2 \cos^2(3\theta'_{nm}). \tag{15}$$

We see that the coupling induced by the anisotropic hyperfine interaction is different in all three spatial directions. Recall that we have labeled our axes such that z, y, and x refer to the translational, circumferential, and radial directions, respectively. We show typical values for A_2^j in Table I. The direction of strongest hyperfine interaction is radial to the nanotube.[55] It is interesting to note the competing signs: the Fermi contact interaction (expressed via A_1) enhances the anisotropic hyperfine interaction along the radial direction, but reduces it along the circumferential and transverse directions. Furthermore, the signs of the hyperfine coupling along different directions indicate ferro- and antiferromagnetic alignment of the nuclear spins with respect to the electron spin (in the ground state). We will come back to this in Sec. IV.

Finally, we address the coupling of electron orbital angular momentum. Calculating matrix elements of h_3^k, it is straightforward to see that this interaction vanishes identically by applying the operators L_j to the hydrogenic orbitals appearing in Eq. (2), then evaluating $\langle \Psi_\sigma | h_3^k | \Psi_{\sigma'} \rangle$ and summing up all contributions.

B. Graphene

We consider the "graphene limit" corresponding to let $n,m \to \infty$ in all expressions in Sec. III A. Then $\beta_{nm} \to 0$ and $N_{nm} \to 1$ and, denoting quantities related to graphene with a tilde,

$$\tilde{A}_1 = 0, \quad \tilde{A}_2^z = \tilde{A}_2^y = -\frac{\tilde{A}_2^x}{2} = -\frac{\mu_0 \gamma_S \gamma^{13}_{\text{C}} Z_{\text{eff}}^3}{240\pi a_0^3}. \tag{16}$$

Inserting numbers, this yields $\tilde{A}_2^z = \tilde{A}_2^y \simeq -0.3$ μeV and $\tilde{A}_2^x \simeq 0.6$ μeV. Note that in our notation the x direction is perpendicular to the graphene plane.

Surprisingly, these numbers are not much different from those estimated for A_2^j in Sec. III A. Naively, one might have expected a weaker hyperfine interaction in graphene (as compared to CNTs) due to its flatness and the vanishing contact interaction (4). As it turns out, however, even for small CNTs the contact interaction is only a small correction to the anisotropic hyperfine interaction (5), so that the latter is the main hyperfine contribution for both CNTs and flat graphene.

IV. HYPERFINE-INDUCED ANISOTROPIC KNIGHT SHIFT

In Secs. II and III, we have formulated the hyperfine problem in terms of a local coordinate system at each nucleus. In this section, we want to look at the Knight shift in the ^{13}C nuclear spins due to hyperfine interaction with the conduction electron. The isotropic Knight shift due to interaction with both the sp-hybridized conduction-band electron and the $1s$ core electron has been studied in Ref. 47. Electron-spin resonance spectra of ^{13}C in π-electron radicals have been analyzed in Ref. 48.

From our considerations in Sec. III A it is clear that the Knight shift induced by the anisotropic hyperfine interaction ($\sim A_2^j/N$) exceeds the isotropic Knight shift ($\sim A_1/N$) by roughly one order of magnitude (N is the number of nuclei in

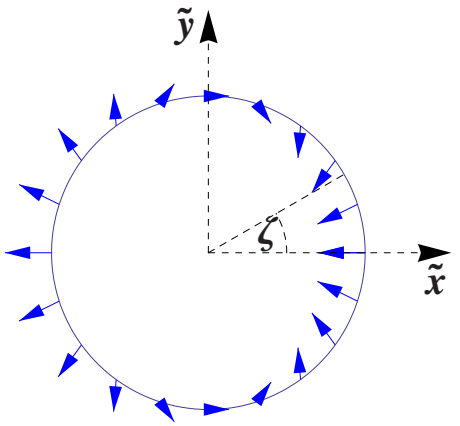

FIG. 3. (Color online) Alignment of the nuclear spins (in the ground state) due to the anisotropic Knight shift. The electron is assumed to be prepared in the eigenstate of $S^{\tilde{x}}$ with eigenvalue $+1/2$, see Eq. (19), and points along $\tilde{x}$ at each nuclear-spin site.

the dot). The Knight shift in CNTs (and graphene) is therefore highly anisotropic.

We introduce the following global coordinate system: $\tilde{x}=x\cos\zeta-y\sin\zeta$, $\tilde{y}=x\sin\zeta+y\cos\zeta$, $\tilde{z}=z$, such that the $\tilde{x}\tilde{y}$ plane cuts out a cross section of the CNT and ζ is the coordinate describing the position on this cross section (see Fig. 3).

The electron is assumed to be prepared in a fixed state and to be delocalized over the CNT cross section. At each lattice point occupied by a ^{13}C nucleus, the nuclear spin will align itself in such a way that the hyperfine energy is minimized in the ground state of the nuclear spins. This ground state can only be achieved for temperatures that are small with respect to the energies associated with the Knight shift: $k_BT<(A_1+A_2^j)/N\sim 1$ peV…1 neV, where k_B is the Boltzmann constant. We write the Hamiltonian describing the hyperfine interaction of one nucleus with the delocalized electron as

$$H'_{\rm hf}=\mathbf{S}^T\mathcal{A}\mathbf{I}=\tilde{\mathbf{S}}^T\tilde{\mathcal{A}}\tilde{\mathbf{I}}, \tag{17}$$

where $\mathbf{S}^T=(S^x,S^y,S^z)$, $\mathcal{A}=\mathrm{diag}(A^x,A^y,A^z)$, $\mathbf{I}=(I^x,I^y,I^z)^T$, $\tilde{\mathbf{S}}^T=\mathbf{S}^TR^\dagger$, $\tilde{\mathcal{A}}=R\mathcal{A}R^\dagger$, and $\tilde{\mathbf{I}}=R\mathbf{I}$, with the rotation R given by

$$R=\begin{pmatrix}\cos\zeta & -\sin\zeta & 0\\ \sin\zeta & \cos\zeta & 0\\ 0 & 0 & 1\end{pmatrix}. \tag{18}$$

The operators carrying a tilde hence describe the interaction in the global coordinate system $(\tilde{x},\tilde{y},\tilde{z})$, and the coupling tensor is given by

$$\tilde{\mathcal{A}}=\begin{pmatrix}A_x\cos^2\zeta+A_y\sin^2\zeta & (A_x-A_y)\sin\zeta\cos\zeta & 0\\ (A_x-A_y)\sin\zeta\cos\zeta & A_x\cos^2\zeta+A_y\sin^2\zeta & 0\\ 0 & 0 & A_z\end{pmatrix}.$$

Here, $A_j=A_1+A_2^j$ is the sum of isotropic and anisotropic hyperfine couplings along the (local) j-direction ($j=x,y,z$), see Eqs. (9) and (12). Recall that $A_x>0$ and $A_y,A_z<0$ for CNTs (see Sec. III A). For an electron spin in an eigenstate of $S^{\tilde{x}}$, the interaction reads

$$H_{\rm hf}^{\tilde{x}}=(A_{\tilde{x}\tilde{x}}I^{\tilde{x}}+A_{\tilde{x}\tilde{y}}I^{\tilde{y}})S^{\tilde{x}} \tag{19}$$

with $A_{\tilde{x}\tilde{x}}=A_x\cos^2\zeta+A_y\sin^2\zeta$ and $A_{\tilde{x}\tilde{y}}=(A_x-A_y)\sin\zeta\cos\zeta$.

In Fig. 3 we show the alignment of the nuclear spins (assuming the nuclear spins to be in their ground state) due to the anisotropic Knight shift induced by the hyperfine interaction with a conduction electron whose spin is prepared in the eigenstate of $S^{\tilde{x}}$ with eigenvalue $+1/2$, i.e., pointing along the $\tilde{x}$ direction at each nuclear site. We have assumed that the electron is evenly distributed around the CNT cross section, which can be seen to be justified from the envelope functions calculated in Ref. 16 for semiconducting CNTs subject to a rectangular confinement potential. We observe an interesting interplay between ferro- and antiferromagnetic coupling along the two spatial directions, which is a direct consequence of the CNT geometry and the strong anisotropy of the hyperfine interaction. In particular, the hyperfine interaction does not vanish when we average over the CNT circumference. This could lead to other interesting effects. For instance, it has been shown in Ref. 49 that in a Luttinger liquid, a nonvanishing average hyperfine field can lead to a transition into a helically ordered phase (along the tube axis) of the nuclear spins below some critical temperature.

V. ELECTRON-SPIN DECOHERENCE

A. Carbon nanotubes

Based on our analysis in Sec. III, the electron-spin dynamics in a CNT are described by the following hyperfine Hamiltonian:

$$H_{\rm hf}=\mathbf{h}\cdot\mathbf{S},\quad h_j=\sum_k A_k^jI_k^j, \tag{20}$$

where $A_k^j=A_jv_0|\Phi(\mathbf{r}_k)|^2$ and $A_j=A_1+A_2^j$, see Eqs. (9) and (12).

We assume that an external magnetic field B_z has been applied along the symmetry axis of the CNT [see Fig. 1(b)], and that the induced Zeeman splitting between the spin states is larger than the hyperfine coupling strength: $b=g\mu_BB_z>A_j$. Assuming $g\simeq 2$, this corresponds to very moderate fields of $B_z\gtrsim 5$ mT. Within this limit, relaxation-induced decoherence is suppressed by the small parameter A_j/b, and the main source of decoherence is pure dephasing due to nuclear-field fluctuations along the CNT symmetry axis. The relevant Hamiltonian is given by the z part of Eq. (20) and the Zeeman term

$$H=(b+h_z)S^z. \tag{21}$$

Assuming that all nuclei carry nonzero spin, the dynamics of the transverse spin is then given by a Gaussian decay with time scale given by $\sqrt{N}/A_z$, where N is the total number of nuclear spins in the quantum dot.[10]

One advantage of carbon-based nanostructures is the low natural abundance of the spin-carrying isotope ^{13}C. In order to investigate this advantage, we allow for arbitrary ^{13}C abundances: we denote the total number of nuclei in the quantum dot (defined via the envelope function, see below) by N, and by N_{12} and N_{13} the number of ^{12}C and ^{13}C nuclei,

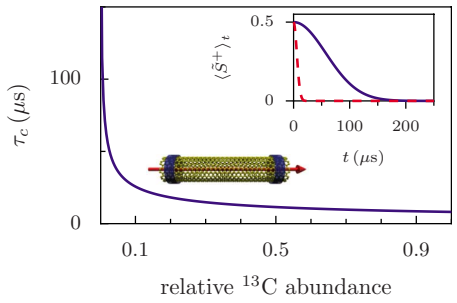

FIG. 4. (Color online) Electron-spin decoherence time τ_c in a (20,0) CNT as a function of the relative ^{13}C abundance N_{13}/N, under the condition of a magnetic field $B_z \gtrsim 5$ mT along the symmetry axis of the CNT. We have chosen a completely unpolarized nuclear system ($p=0$) and $N=6\times10^5$, see text below Eq. (23). Inset: electron-spin dynamics in CNTs with ^{13}C abundances of 1% (solid blue curve) and 99% (dashed red curve), in the frame rotating with $\omega+pN_{13}$, see Eq. (22).

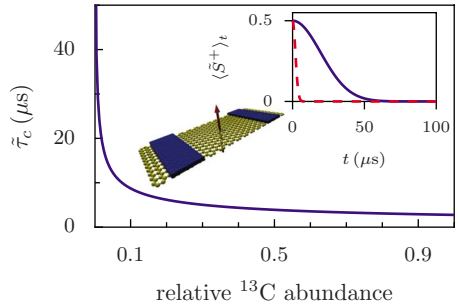

FIG. 5. (Color online) Electron-spin decoherence time $\tilde{\tau}_c$ in graphene as a function of the relative ^{13}C abundance N_{13}/N, under the condition of a magnetic field $B_x \gtrsim 5$ mT perpendicular to the graphene plane. We have chosen $p=0$ and $N=4\times10^5$ (see text in Sec. V B). Inset: electron-spin dynamics in graphene with ^{13}C abundances of 1% (solid blue curve) and 99% (dashed red curve), in the rotating frame.

respectively, such that $N=N_{12}+N_{13}$. This generalization has two relevant effects: (i) summing over all N nuclei, we get $\Sigma_k A_k^z = \eta A_z$, i.e., the total hyperfine coupling is weakened by the ratio $\eta=N_{13}/N$. (ii) The polarization p of the nuclear-spin system ($0\le p\le 1$) is determined only by the distribution of spin-up and spin-down ^{13}C nuclei, while being unaffected by the ^{12}C nuclei.

For $N_{13}\gg 1$ we can use the central limit theorem (compare with Ref. 10) which yields the following Gaussian dynamics for the transverse electron spin [written in the frame rotating with frequency $(\omega+p\eta A_z/2)/\hbar$, where $\omega=b-b_N$ with the nuclear Zeeman energy $b_N=g_N\mu_N B_z$]:

$$\langle S^+ \rangle_t = \langle S^+ \rangle_0 e^{-t^2/\tau_c^2}. \tag{22}$$

Here, $S^+=S^x+iS^y$, with the electron-spin operators $S^j=\sigma_j/2$ and the Pauli operators σ_j. The characteristic time scale for the decay is given by[10]

$$\tau_c = \frac{2\hbar}{\sqrt{1-p^2}} \frac{N}{\sqrt{N_{13}} A_z}. \tag{23}$$

We can see from Eq. (23) that the decoherence time τ_c has an interesting nonlinear dependence on the abundance of ^{13}C nuclei.

The total number N of nuclei in the quantum dot is determined by the quantum-dot confinement. Assuming a rectangular confinement along the symmetry axis[16] and a (20,0) CNT of length 300 nm, we estimate $N\simeq 6\times10^5$. We show the electron-spin decoherence time τ_c as a function of the relative ^{13}C abundance in Fig. 4 for a completely unpolarized nuclear bath ($p=0$). We see that decoherence times of several tens of microseconds can be expected for higher ^{13}C abundances. For the natural ^{13}C abundance of about 1%, we estimate $\tau_c \gtrsim 200$ μs from Eq. (23). The inset of Fig. 4 shows the Gaussian decay of the spin coherence (Eq. (22)) for CNTs containing 1% (solid line) and 99% (dashed line) ^{13}C nuclei. We note that further increase in the decoherence time τ_c, say by a factor of x, would require isotopic purification and the reduction in the natural ^{13}C abundance by about a factor of x^2. The decoherence law in Eqs. (22) and (23) of course breaks down at the point when only a few nuclear spins are present in the dot.

B. Graphene

For an electron confined to a graphene quantum dot, the contact interaction vanishes identically [$\tilde{A}_1=0$, see Eq. (16)], and only the anisotropic hyperfine interaction contributes to spin decoherence. We assume an externally applied magnetic field B_x perpendicular to the graphene plane [see Fig. 1(a)], giving rise to a Zeeman splitting $\tilde{b}=g_\perp \mu_B B_x$, where $g_\perp \simeq 2$ is the electron g factor in the out-of-plane direction. If the Zeeman splitting is much larger than the energy associated with the transverse hyperfine terms, $\tilde{b} \gg \tilde{A}_2^z, \tilde{A}_2^y$, the electron-spin dynamics are governed by a Gaussian decay similar to the CNT case (22), but with a characteristic time scale given by

$$\tilde{\tau}_c = \frac{2\hbar}{\sqrt{1-p^2}} \frac{N}{\sqrt{N_{13}} \tilde{A}_2^x}. \tag{24}$$

For a quantum dot with width $W=30$ nm and length $L=30$ nm, we estimate the total number of nuclei to be $N\simeq 4\times10^5$. We show $\tilde{\tau}_c$ as a function of the relative ^{13}C abundance in Fig. 5: for higher ^{13}C abundances, decoherence times $\tilde{\tau}_c \gtrsim 1$ μs can be expected, while for the natural ^{13}C abundance of 1%, we estimate $\tilde{\tau}_c \gtrsim 80$ μs.

C. Comparison and discussion

It is interesting to note that the electron-spin decoherence times in graphene are shorter than in CNTs. Naively, one would assume that the CNT curvature and the associated hybridization would lead to an enhancement of the nuclear-spin interactions due to the contact interaction (4). As it turns out, however, the contact interaction in a CNT has a competing sign as compared to the anisotropic hyperfine interaction along the CNT symmetry axis and, hence, effectively reduces the total hyperfine coupling strength along the direction of the external magnetic field. For ultrasmall CNTs it might happen that the total hyperfine coupling along the

TABLE II. Comparison of our hyperfine coupling strengths with the values from previous publications for comparable systems. We give our values for a (20,0) zigzag nanotube and for graphene. See Sec. VI for a detailed discussion.

	A_1 (μeV)	A_2^x (μeV)	$A_2^{y,z}$ (μeV)
Our values (CNT)	0.05	0.6	−0.3
Our values (Graphene)	0	0.6	−0.3
Yazyev[b] (Graphene flakes)	−0.2	0.6	−0.3
Pennington, Stenger[a] (C_{60})	0.1	0.9	−0.5
Goze-Bac *et al.*[c] (CNT)	0.04	0.9	−0.5

[a]Reference 36.
[b]Reference 37.
[c]Reference 50.

symmetry axis approaches zero.[56] This, however, is beyond the validity of our theory.

For typical CNTs, the dominant contribution to the nuclear-spin interactions in CNTs comes from the anisotropic hyperfine interaction. This is because the amount of *s*-orbital admixture in the hybridized wave function of a conduction-band electron is rather small: on the order of a few percent.

In our considerations throughout this section, we have neglected the hyperfine terms which are transverse to the externally applied magnetic field, i.e., radial and circumferential in the case of a CNT, and in-plane in the case of graphene. This gives a good first approximation of the decoherence time, as long as the external magnetic field is large enough to suppress spin flips induced by the hyperfine terms transverse to the external field. For both CNTs and graphene, magnetic fields of order $B \gtrsim 5$ mT are sufficiently strong to achieve this.

VI. COMPARISON WITH PREVIOUS WORK

In Table II we compare our results for the hyperfine interaction in graphene and CNTs with those given in earlier publications for comparable systems. Yazyev's values[37] for the hyperfine interactions in small graphene flakes were derived from DFT calculations including the σ bands. The values for the anisotropic hyperfine interaction are similar to our results but a nonvanishing (and even negative) value for the isotropic hyperfine interaction is reported, which is, however, associated with the coupling between the nuclear spins and the 1*s* core electrons, which is irrelevant for the dephasing of the conduction electron. Pennington and Stenger[36] give estimates for the hyperfine interaction in fullerenes and report coupling constants which are slightly larger than our values. The relatively large value for the isotropic hyperfine interaction can be explained by the stronger curvature in C_{60} molecules, leading to stronger *sp*-hybridization of the electron states, as compared to CNTs. Goze-Bac *et al.*[50] have estimated the hyperfine interaction in CNTs based on measurements of the chemical shift in ^{13}C.

Churchill *et al.*[34] have estimated the hyperfine interaction in carbon nanotubes from transport measurements in double quantum dots, but do not comment on the anisotropy of the interaction. A hyperfine coupling strength of ~ 100 μeV for pure ^{13}C CNTs is reported in their work, in clear contrast to our results. Currently, this discrepancy is not understood. One possible explanation[51] for this might be that the theory developed in Ref. 52 for standard GaAs quantum dots and used in Ref. 34 to deduce the hyperfine coupling strength gets modified by the valley degeneracy occurring in CNT and thus this could lead to different conclusions. Another possible explanation[34] could be that the effective electron-nuclear interaction gets greatly enhanced by electron-electron interactions and the one-dimensional character of the system. A similar renormalization was recently noticed in the context of nuclear magnetic ordering in CNT.[49] Clearly, this is an interesting open problem, which, however, requires separate study.

VII. CONCLUSIONS

We have calculated the nuclear-spin interactions and the resulting spin dynamics of an electron confined to a CNT or graphene quantum dot. In graphene, only the anisotropic hyperfine interaction couples the electron to the nuclear spins, due to the purely *p*-type electron wave function. In a CNT, curvature induces an *sp*-hybridization of the electron orbital, opening a new channel of spin decoherence via the Fermi contact interaction. However, for typical CNTs, the Fermi contact interaction is only a small correction to the anisotropic hyperfine interaction, the latter being the main source of nuclear-spin-induced decoherence of the electron spin. We found the total hyperfine coupling strength of an electron with the ^{13}C nuclei to be less than 1 μeV for both graphene and CNTs quantum dots—about two orders of magnitude smaller than the hyperfine interaction of an electron in a GaAs or InAs quantum dot.

We have used a simple model for the *sp*-hybridization in CNTs, from which we have derived the hyperfine interaction. We have checked, however, that a numerical tight-binding band structure calculation yields hybridization on the same order of magnitude as the geometrical approach used in this work.[53] Nevertheless, a more rigorous band structure calculation including also the influence of the CNT σ bands would be desirable in the future.

For CNTs, we have found an interesting interplay of hyperfine couplings along different spatial directions, leading to a highly anisotropic Knight shift and an alignment of the ^{13}C nuclear spins around the CNT in the ground state of the nuclear spins. This result is particularly interesting when viewed in context of the hyperfine-induced nuclear phase transition predicted in Ref. 49 for a Luttinger liquid, which requires a nonvanishing mean value of the hyperfine field. The strong anisotropy of the hyperfine field that we have found in our work thus gives further evidence that such phase transitions could occur in CNTs. We emphasize that this anisotropy is present in CNTs of any chirality, in particular also in metallic CNTs. The results presented here have been used very recently in the context of transport though CNT quantum dots.[44]

Furthermore, we have estimated typical electron-spin decoherence times in CNT and graphene quantum dots. We

have shown that relaxation-induced decoherence due to nuclear spins can be suppressed by applying a magnetic field of order 5 mT to the system, leaving only pure dephasing due to fluctuations of the nuclear magnetic field. We have estimated that for a (20,0) zigzag CNT quantum dot containing $N \simeq 6 \times 10^5$ nuclei, and for a magnetic field applied along the CNT symmetry axis, the associated decoherence time is of order $\tau_c \gtrsim 1$ μs, depending on the relative ^{13}C abundance. We emphasize that our analytical treatment of the hyperfine problem applies to CNTs of any chirality. For a graphene quantum dot containing $N=4 \times 10^5$ nuclei, and for a magnetic field applied perpendicular to the graphene plane, the decoherence time is of order $\tilde{\tau}_c \gtrsim 0.5$ μs, again depending on the relative ^{13}C abundance.

The hyperfine interaction in the systems we have considered here is rather weak. Therefore, it could, in principle, be that other mechanisms, such as spin-orbit interactions, limit the lifetime of spin-state superpositions on time scales comparable to those we have estimated here (see Ref. 16 for details).

The decoherence times we have estimated throughout this work are among the longest reported so far. This makes quantum dots based on carbon materials attractive spin-qubit candidates. In particular, the tunability of the average hyperfine coupling strength via the abundance of spin-carrying ^{13}C nuclei could be used to achieve an optimal balance between a long electron-spin decoherence time and a sufficiently strong coupling to control the electron-spin state by manipulating the nuclear-spin system.

ACKNOWLEDGMENTS

We acknowledge useful discussions with B. Braunecker, J. Klinovaja, M. J. Schmidt, and D. Stepanenko, and funding from the Swiss NSF, NCCR Nanoscience, JST ICORP, DARPA Quest, QuantumWorks, and the German DFG.

[1] D. D. Awschalom, D. Loss, and N. Samarth, *Semiconductor Spintronics and Quantum Computing* (Springer-Verlag, Berlin, 2002).
[2] I. Žutić, J. Fabian, and S. Das Sarma, Rev. Mod. Phys. **76**, 323 (2004).
[3] D. D. Awschalom and M. E. Flatte, Nat. Phys. **3**, 153 (2007).
[4] D. Loss and D. P. DiVincenzo, Phys. Rev. A **57**, 120 (1998).
[5] V. Cerletti, W. A. Coish, O. Gywat, and D. Loss, Nanotechnology **16**, R27 (2005).
[6] R. Hanson, L. P. Kouwenhoven, J. R. Petta, S. Tarucha, and L. M. K. Vandersypen, Rev. Mod. Phys. **79**, 1217 (2007).
[7] G. Burkard, D. Loss, and D. P. DiVincenzo, Phys. Rev. B **59**, 2070 (1999).
[8] I. A. Merkulov, A. L. Efros, and M. Rosen, Phys. Rev. B **65**, 205309 (2002).
[9] A. V. Khaetskii, D. Loss, and L. Glazman, Phys. Rev. Lett. **88**, 186802 (2002).
[10] W. A. Coish and D. Loss, Phys. Rev. B **70**, 195340 (2004).
[11] A. C. Johnson, J. R. Petta, J. M. Taylor, A. Yacoby, M. D. Lukin, C. M. Marcus, M. P. Hanson, and A. C. Gossard, Nature (London) **435**, 925 (2005).
[12] F. H. L. Koppens, J. A. Folk, J. M. Elzerman, R. Hanson, L. H. W. van Beveren, I. T. Vink, H. P. Tranitz, W. Wegscheider, L. P. Kouwenhoven, and L. M. K. Vandersypen, Science **309**, 1346 (2005).
[13] Ł. Cywiński, W. M. Witzel, and S. Das Sarma, Phys. Rev. Lett. **102**, 057601 (2009).
[14] J. R. Petta, A. C. Johnson, J. M. Taylor, E. A. Laird, A. Yacoby, M. D. Lukin, C. M. Marcus, M. P. Hanson, and A. C. Gossard, Science **309**, 2180 (2005).
[15] B. Trauzettel, D. V. Bulaev, D. Loss, and G. Burkard, Nat. Phys. **3**, 192 (2007).
[16] D. V. Bulaev, B. Trauzettel, and D. Loss, Phys. Rev. B **77**, 235301 (2008).
[17] S. Schnez, F. Molitor, C. Stampfer, J. Guettinger, I. Shorubalko, T. Ihn, and K. Ensslin, Appl. Phys. Lett. **94**, 012107 (2009).
[18] L. A. Ponomarenko, F. Schedin, M. I. Katsnelson, R. Yang, E. W. Hill, K. S. Novoselov, and A. K. Geim, Science **320**, 356 (2008).
[19] S. J. Tans, M. H. Devoret, H. Dai, A. Thess, R. E. Smalley, L. J. Geerligs, and C. Dekker, Nature (London) **386**, 474 (1997).
[20] M. Bockrath, D. H. Cobden, P. L. McEuen, N. G. Chopra, A. Zettl, A. Thess, and R. E. Smalley, Science **275**, 1922 (1997).
[21] J. Kong, C. Zhou, E. Yenilmez, and H. Dai, Appl. Phys. Lett. **77**, 3977 (2000).
[22] E. D. Minot, Y. Yaish, V. Sazonova, and P. L. McEuen, Nature (London) **428**, 536 (2004).
[23] P. Jarillo-Herrero, S. Sapmaz, C. Dekker, L. P. Kouwenhoven, and H. S. J. van der Zant, Nature (London) **429**, 389 (2004).
[24] N. Mason, M. J. Biercuk, and C. M. Marcus, Science **303**, 655 (2004).
[25] M. J. Biercuk, S. Garaj, N. Mason, J. M. Chow, and C. M. Marcus, Nano Lett. **5**, 1267 (2005).
[26] J. Cao, Q. Wang, and H. Dai, Nature Mater. **4**, 745 (2005).
[27] S. Sapmaz, C. Meyer, P. Beliczynski, P. Jarillo-Herrero, and L. P. Kouwenhoven, Nano Lett. **6**, 1350 (2006).
[28] E. Onac, F. Balestro, B. Trauzettel, C. F. J. Lodewijk, and L. P. Kouwenhoven, Phys. Rev. Lett. **96**, 026803 (2006).
[29] M. R. Gräber, W. A. Coish, C. Hoffmann, M. Weiss, J. Furer, S. Oberholzer, D. Loss, and C. Schönenberger, Phys. Rev. B **74**, 075427 (2006).
[30] H. I. Jørgensen, K. Grove-Rasmussen, J. R. Hauptmann, and P. E. Lindelof, Appl. Phys. Lett. **89**, 232113 (2006).
[31] C. Meyer, J. M. Elzerman, and L. P. Kouwenhoven, Nano Lett. **7**, 295 (2007).
[32] F. Kuemmeth, S. Ilani, D. C. Ralph, and P. L. McEuen, Nature (London) **452**, 448 (2008).
[33] G. A. Steele, G. Gotz, and L. P. Kouwenhoven, Nat. Nanotechnol. **4**, 363 (2009).
[34] H. O. H. Churchill, A. J. Bestwick, J. W. Harlow, F. Kuemmeth, D. Marcos, C. H. Stwertka, S. K. Watson, and C. M. Marcus, Nat. Phys. **5**, 321 (2009).
[35] H. O. H. Churchill, F. Kuemmeth, J. W. Harlow, A. J. Bestwick, E. I. Rashba, K. Flensberg, C. H. Stwertka, T. Taychatanapat, S.

K. Watson, and C. M. Marcus, Phys. Rev. Lett. **102**, 166802 (2009).
[36] C. H. Pennington and V. A. Stenger, Rev. Mod. Phys. **68**, 855 (1996).
[37] O. V. Yazyev, Nano Lett. **8**, 1011 (2008).
[38] R. Saito, G. Dresselhaus, and M. S. Dresselhaus, *Physical Properties of Carbon Nanotubes* (Imperial College Press, London, 1998).
[39] A. Kleiner and S. Eggert, Phys. Rev. B **64**, 113402 (2001).
[40] J. Fischer, W. A. Coish, D. V. Bulaev, and D. Loss, Phys. Rev. B **78**, 155329 (2008).
[41] E. Clementi and D. L. Raimondi, J. Chem. Phys. **38**, 2686 (1963).
[42] A. M. Stoneham, *Theory of Defects in Solids* (Oxford University Press, London, 1975), Chap. 13.
[43] S. Latil, L. Henrard, C. Goze Bac, P. Bernier, and A. Rubio, Phys. Rev. Lett. **86**, 3160 (2001).
[44] A. Pályi and G. Burkard, arXiv:0908.1054 (unpublished).
[45] D. Paget, G. Lampel, B. Sapoval, and V. I. Safarov, Phys. Rev. B **15**, 5780 (1977).
[46] Y. G. Semenov, K. W. Kim, and G. J. Iafrate, Phys. Rev. B **75**, 045429 (2007).
[47] O. V. Yazyev and L. Helm, Phys. Rev. B **72**, 245416 (2005).
[48] M. Karplus and G. K. Fraenkel, J. Chem. Phys. **35**, 1312 (1961).
[49] B. Braunecker, P. Simon, and D. Loss, Phys. Rev. Lett. **102**, 116403 (2009).
[50] C. Goze-Bac, S. Latil, P. Lauginie, V. Jourdain, J. Conard, L. Duclaux, A. Rubio, and P. Bernier, Carbon **40**, 1825 (2002).
[51] B. Trauzettel and D. Loss, Nat. Phys. **5**, 317 (2009).
[52] O. N. Jouravlev and Y. V. Nazarov, Phys. Rev. Lett. **96**, 176804 (2006).
[53] M. J. Schmidt (private communication).
[54] For typical CNTs we have $2\pi/L < 1$. However, the parameter can approach unity for ultrasmall nanotubes. At this point, our theory breaks down.
[55] The fact that $A_2^x \simeq -2A_2^y \simeq -2A_2^z$ for the CNTs in Table I comes directly from the angular integration in the expressions $\langle \Psi_\sigma | h_2^k | \Psi_{\sigma'} \rangle$, leading to Eq. (11): the admixture of ψ_{2p_t} and ψ_{2p_c} to the π orbital in Eq. (2) is very small, such that the integration approximately reduces to the $\psi_{2p_\perp}$ term (the ψ_{2s} term does not contribute by symmetry).
[56] We emphasize that this result is different from Refs. 46 and 47, where only the isotropic hyperfine interactions of the nuclear spins with the 1*s* and 2*s* electrons have been considered.